# Computational and biological efficacy of stigmasterol against HeLa cells and Vero cells- first time isolated from the ethanolic extract of *Annonamuricata* Linn leaves

J. Irshad Ahamed [a,*], Francy K [a], A. Vini Priya [b], J. PremaKumari [c], R.P. Steiny [d], P. Kamalarajan [e], B. Venkatadri [f]

[a] Department of Chemistry, Scott Christian College (Autonomous), Nagercoil-629 003, Reg. No: 18223162032028, Research Scholar, Manonmaniam Sundaranar University, Abisekapatti, Tirunelveli, Tamil Nadu, India
[b] Department of Chemistry, Government Arts College for Women, Ramanathapuram, Tamil Nadu, India
[c] Department of Chemistry and Research Centre, Scott Christian College (Autonomous), Nagercoil 629 003, Tamil Nadu, India
[d] Department of Chemistry, Central University of Tamilnadu, Thiruvarur, Tamil Nadu, India
[e] Department of Chemistry, R.M.D Engineering College, Kavaraipettai, Tamil Nadu 601206, India
[f] Department of Plant Biology and Biotechnology, Loyola College (Autonomous), Affiliated to University of Madras, Chennai 600034, Tamil Nadu, India

## ARTICLE INFO

## ABSTRACT

The present study was aimed to analyze the *in vitro* antioxidant, anti-inflammatory and cytotoxicity activities of isolated bioactive compound stigmasterol (abbreviated as STML) from the leaves of *Annonamuricata*. Extraction was done using Soxhlet apparatus, TLC, column chromatography and STML in the extracts were identified by Gas-Chromatography and Mass-Spectroscopy (GC–MS) analyses. Characterizations of isolated bioactive compound stigmasterol for purity verified were performed using High-performance liquid chromatography (HPLC) technique. Stigmasterol compound was estimated by DPPH scavenging and ABTS assay, it showed significant values. *In vitro* cytotoxicity activity of stigmasterol was also tested HeLa cells and Vero cells and $IC_{50}$ values found that 11.58 µg/ml and 173.8 µg/ml, respectively. The different spectral analysis were also characterized by experimental and well deal with the theoretical *ab* initio Density functional theory (DFT) method at B3LYP level with $6-311++G$(d,p) basis set of provides for the different spectral studies, respectively by using UV-Visible,[1]Hand ^{13}C nuclear magnetic resonance (NMR) spectroscopy studies. Fourier-transform infrared (FTIR) spectral analysis was carried out. Density Function Theory (DFT) computations enabled us to get different reactive properties of STML. The Rf of STML isolated from the ethanolic extracts of *Annonamuricata* leaves is 3.707. In conclusion, the results suggest that the investigated compounds are potential drug leads to target HeLa cells and Vero cells.

© 2021 Elsevier B.V. All rights reserved.

## 1. Introduction

Each year, more than 500,000 women are diagnosed with the deadly cause of cervical cancer. This disease, which is projected inside the vagina, is the fourth most frequent malignancy in women, and it is linked to the human papillomavirus (HPV) [1–4]. Treatment is determined by the stage of cancer, and many therapies, such as radiation, chemotherapy, or immunotherapy, may be used [5]. Cisplatin, carboplatin, paclitaxel, topotecan, and gemcitabine are the most often used drugs to treat cervical cancer. However, numerous side effects have been connected with the usage of these

treatments [6]. Furthermore, the expensive price of the therapies makes them inaccessible to the general public [7]. As a result, it is critical to look for new therapies that are less expensive and do not have negative effects. One of these alternatives is the employ of bioactive compounds from natural sources and, therefore, takes benefit of the biological wealth of developing countries [8].

STML is a natural 6–6–6–5 tetracyclic phytosterol, which constitutes a rigid tetracyclic backbone with one hydroxyl group at one end and one C10 branched hydrocarbon chain at the other end. It has been inspected for its pharmacological prospects, such as cytotoxic, antitumor, antimutagenic, antioxidant, anti-inflammatory, and CNS effects [9]. In our current research, STML was isolated from the leaves of *Annona muricata.* As far as we know, STML is the first report on the isolation of stigmasterol from the leaves of *Annona muricat.* Different spectral analysis, DFT-computational,

* Corresponding author at: Department of Chemistry (SHIFT – II), C. Kandaswami Naidu College for Men, Anna Nagar East, Chennai, Tamil Nadu 600102, India.
*E-mail addresses:* irshad@loyolacollege.edu, irshadckncchembio@gmail.com (J.I. Ahamed).

and *in silico* molecular docking studies were completed for this STML compound. This density functional theory (DFT) calculation study has a diversity of both experimental and theoretical data, and revealed enhanced binding interactions in docking analysis. This isolated compound STML has exhibited potent anticancer activities against HeLa cell lines at different concentrations. So, we are promising that the results of this study can guide the design of structural analysis, quantum chemical studies on molecular geometry, chemical reactivity, and new biological evolutions by the researchers.

## 2. Materials and methods

### 2.1. Purchase chemicals and reagents

Petroleum ether, Chloroform, Hexane, Ethanol, ceric ammonium nitrate, DPPH solution, Ascorbic acid, Methanol, chloroform, acetic anhydride, Silica gel 60–120 mesh and TLC silica gel 60 ready-made plates were obtained from Merk, USA. Column of size 90 cm × 2.5 cm was used. ABTS, Potassium persulfate, myoglobulin were obtained from Sigma, USA. 0.1 mM DPPH solution, Ascorbic acid, Methanol, Dissolve 39 mg of DPPH in 100 ml of methanol and store at −20 °C until needed, 1 mg/ ml of Ascorbic acid. Acetyl salicylic acid, BSA was purchased from Sigma Aldrich, USA. 10X PBS were purchased from Himedia, India. DMEM medium and Fetal Bovine Serum (FBS) and antibiotic solution were from Gibco (USA), DMSO (Dimethyl sulfoxide) and MTT (3–4,5 dimethylthiazol-2yl-2,5-diphenyl tetrazolium bromide) (5 mg/ml) were from Sigma, (USA), RPMI medium, 1X PBS, LSM were from Himedia, (India). 96 well tissue culture plate and wash beaker were purchased from Tarson (India). DMEM medium, Penicillin/Streptomycin antibiotic solution, Trypsin-EDTA was purchased from Gibco (USA), The Alexa Fluor® 488 annex in V/Dead Cell Apoptosis Kit was purchased from Thermo scientific (USA). Fluorescence microscope with fluorescence.

### 2.2. Sample collection and authentication

Plant leaves were collected from Holy Cross College campus, Nagercoil, Tamilnadu, India. Herbarium sheets were prepared for the collected sample. The plant was acknowledged and authenticated in the Botany research herbarium at St.Xavier's college, Palayamkottai, Tamilnadu, India. A voucher specimen was placed in the herbarium under the collection number XCH40369. The leaves were washed well, shade dried, powdered using the mechanical grinder, and preserved for further research.

### 2.3. Extraction and isolation

The isolation was done following the process of [10] with slight modifications. 1000 g of powdered leaf sample of *A. muricata* was subjected to extraction using ethanol at 70 °C for 40 hours in the Soxhlet apparatus. The extracted matter was evaporated under reduced pressure in a rotary evaporator to recover the solvent and to maintain the important ingredients. The resulting crude extracts were subjected to column chromatography. The dried ethanol crude sample was placed to top of the silica column made by wet packing method. The elution was done using chloroform, hexane, methanol and ethanol. Each 10 ml fractions were received and further analyzed by TLC. The fractions with related Rf values were joint into 20 fractions and dried under rotary vacuum evaporator. The 13th fraction with single spot and high quantity was chromatographed for isolation. The isolate was subjected to HPLC [11], GC-MS [12], and UV-Visible, FTIR, ^{13}CNMR and ^{1}H NMR to establish its structure.

### 2.4. Test for alcohol

On moderate heating, 4 g of ceric ammonium nitrate is dissolved in 10 mL of 2 N $HNO_3$. In 0.5 mL of dioxane, a few crystals of the sample are dissolved. The solution was mixed with 0.5 mL of ceric ammonium nitrate reagent, diluted to 1 mL with dioxane, and well shaken. The color of the solution changes from yellow to red. [13].

### 2.5. Salkowski reaction

When chloroform solution of the sample is treated with few drops of Con.$H_2SO_4$, a reddish color is noted in the upper chloroform layer [14].

### 2.6. Libermannburchard reaction

When chloroform solution of the sample is treated with few drops of Con.$H_2SO_4$ followed by the addition of 2–3 drops of acetic anhydride. Solution turns to violet blue and finally green [15].

### 2.7. Spectral characterizations

Rotary vacuum evaporator was utilized to dry the extract. ^{13}C NMR, GC-MS analysis was completed on a GC-MS equipment. Clarus 500 Perkin- Elmer Gas Chromatograph equipped and coupled to a mass detector Turbo mass ver. 5.2 – Perkin Elmer Turbo mass 5.2 spectrometer with an Elite-(5% Phenyl 95% dimethylpolysiloxane), 30 m, and 250 μm capillary columns was used. Shimadzu UV- 1800 and Shimadzu IR Affinity-spectrophotometers were used to record UV and FTIR spectrum respectively. ^{13}C and ^{1}HNMR spectra were recorded in Bruker 300 MHz FT-NMR spectrometer using $CDCl_3$ as solvent. Elemental analysis was completed on the PerkinElmer CHNS/O 2400 series II elemental analyzer (India). Elemental (CHNS/O) analysis specified that the calculated and found values were within the acceptable limits ($\pm 0.4\%$). The HPLC system (Shimadzu) was used,

### 2.8. Computational details

The optimization of the ground state of isolated STML molecule was computed by DFT methods using the Gaussian 09 package [16] at The Becke's three parameter Lee-Yang-Parr hybrid exchange-correlation (B3LYP) functions are utilized in this analysis with $6-311++G$ (d,p) basis set [17–19] for optimization of compounds in the gas phase. Frequency calculation has been done at the same level of theory for the confirmation of the global minima. The theoretical UV-Visible electronic transition properties like the maximum excitation wavelength ($\lambda_{max}$) and oscillator strengths (*f*) spectrum were obtained by performing the TD-DFT method [20,21]. The Gauss Sum 3.0 program has been used to obtain calculated UV-Visible spectrum images [22]. The chemical shifts of the molecule in ^{1}H and ^{13}C nuclear magnetic resonance (NMR) were calculated using the gage independent atomic orbital (GIAO) theory in mixture with B3LYP/$6-311++G$(d,p) and evaluated with experimental outcome. Mulliken charges and chemical reactivity studies are also used to explain the energy of frontier molecular orbitals (HOMO-LUMO). Theoretical simulations were used to determine the characteristics of the molecular electrostatic potential (MEP).

### 2.9. ABTS (2,2′-azino-bis(3-ethylbenzthiazoline-6-sulfonic acid) assay

The total antioxidant capacity of the extracts was determined using ABTS radical. The viable solution was then made by combining equal parts of the two stock solutions and allowing them to

react for 14 h at room temperature in the dark [23]. Using a spectrophotometer, the solution was diluted by mixing 1 ml ABTS solution with 60 ml methanol to produce absorbance of 0.706 ± 0.01 units at 734 nm. For each test, a new ABTS solution was produced. After allowing 1 ml of ST samples to react with 1 ml of ABTS solution for 7 min, the absorbance was measured at 734 nm using a spectrophotometer. The extract ABTS scavenging capacity was compared to that of ascorbic acid, and percentage inhibition was calculated as Abs control BTS radical scavenging activity (%)=Abs control-Abs sample/Abscontrol, where $Abs_{control}$ is the absorbance of the ABTS radical in methanol and Abs sample is the absorbance of the ABTS radical solution mixed with the sample extract/standard. All measurements were made in triplicate (in $n$ = 3).

### 2.10. DPPH radical scavenging activity

The free radical degrading activities of natural bioactive compound of Stigmasterol sample was calculated by a DPPH method. Functional Stigmasterol compound at varying concentrations (500, 400, 300, 200, 100, 50, 15, 10, 5 and 1 µg/mL) was resolute using DPPH as per the method of [24]. Percentage (%) DPPH degrading properties of Stigmasterol sample, and functional Stigmasterol sample were calculated as mentioned below:

$$\text{DPPH scavenging capacity }(\%) = \left[\left(A_{sample} - A_{blank}\right)/A_{control}\right] \times 100$$

#### 2.10.1. Anti-inflammatory activity—Inhibition of albumin denaturation

Protein denaturation is the primary cause of inflammation. The technique of [25,26] with minor modifications was used to assess protein denaturation inhibition. 500 µL of 1% bovine serum albumin was mixed to isolated compound of Stigmasterol (100, 90, 70, 50, 30, 15, 10, 5, 1 and 0.5 µg/mL) of test sample. This mixture was kept at room temperature for 10 min, followed by heating at 51 °C for 20 min. Acetyl salicylic acid was taken as a positive control. The experiment was performed in triplicates and% inhibition for protein denaturation was calculated using the following formula and the statistical analysis was carried out using Graph Pad Prism Software 6.0, USA.

$$\%\text{ Inhibition} = 100 - ((A1 - A2)/A0 * 100)$$

where A1 is the absorbance of the sample, A2 is the absorbance of the product control and A0 is the absorbance of the positive control. A dose response curve was plotted to determine the $IC_{50}$ values. $IC_{50}$ is defined as the concentration enough to reach 50% of a maximum scavenging capacity. All tests and analysis were run in triplicate in addition to averaged.

### 2.11. Anticancer activity

Cervical cancer cells (HeLa) and Vero cells (L-929) were procured from National center for Cell Science, Pune, India. The anticancer activity of isolated compound Stigmasterol (STML) against cervical cancer cells (HeLa) and Vero cells (L-929) were evaluated using MTT [3-(4,5-dimethylthiazol-2-yl)−2,5- diphenyltetrazolium bromide] assay [27]. The optical density (OD) was read and also the cell viability (%) was calculated utilize the following formula:

$$\text{Percentage inhibition }(\%) \left[\left(OD_{control} - OD_{sample}/OD_{control}\right)\right] \times 100.$$

### 2.12. Molecular docking

The current work, molecular docking study was done for protein associated with cervical cancer (HeLa) cell lines investigations. The Multidentate small-molecule inhibitors of vaccinia H1-related (VHR) phosphatase decrease proliferation of cervix cancer cells (RCSB PDB ID: 3F81) was obtained and downloads from RCSB
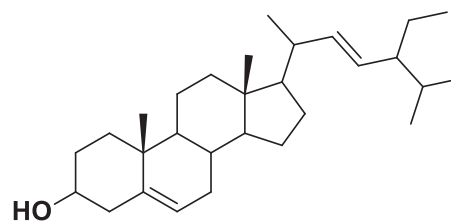


**Fig. 1.** Compound (STML) isolated from the leaves of *Annona muricata*.

**Table 1**
The list of solvent combinations used in column chromatography.

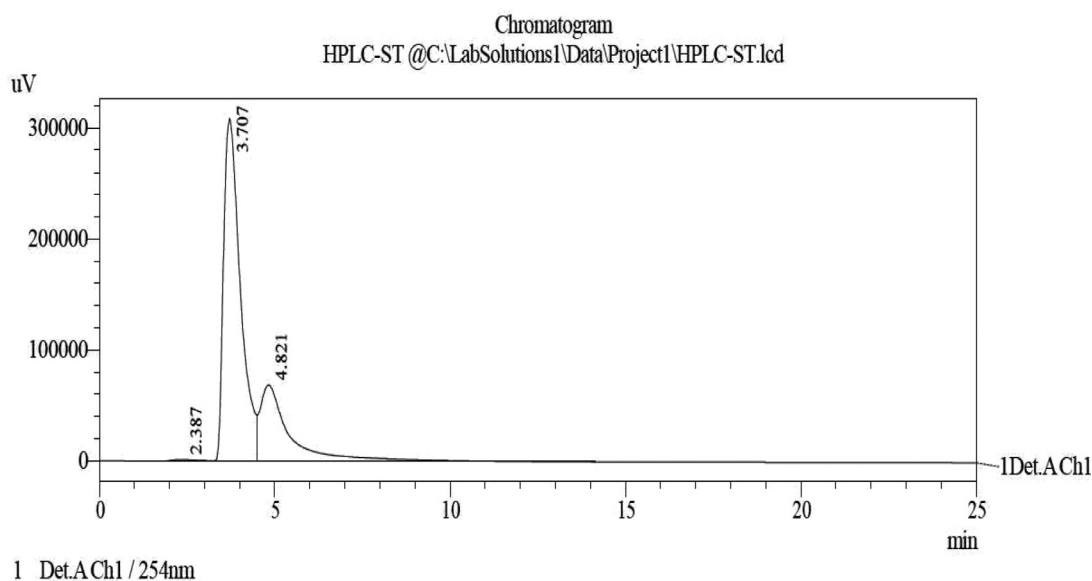| S. No | Solvent system | Ratio | Volume (ml) | Fractions |
|-------|----------------|-------|-------------|-----------|
| 1. | Ethanol | 100% | 20 | 1–2 |
| 2. | Ethanol: Chloroform | 9:1 | 20 | 3–4 |
| 3. | Ethanol: Chloroform | 5:5 | 20 | 5–6 |
| 4. | Ethanol: Chloroform:Hexane | 3:2:5 | 20 | 7–8 |
| 5. | Ethanol: Hexane | 5:5 | 20 | 9–10 |
| 6. | Hexane | 100% | 20 | 11–12 |
| 7. | Ethanol: Chloroform:Hexane | 3:2:5 | 20 | 13–14 |
| 8. | Ethanol:Chloroform | 5:5 | 20 | 15–16 |
| 9. | Ethanol:Chloroform | 9:1 | 20 | 17–18 |
| 10 | Methanol | 100% | 20 | 19–20 |

PDB formatted target protein [28]. This protein is classified with a use of both (hydrolase) in addition to organism of Homo sapiens. Molecular docking studies were completed by Autodock4.2. The docking studies were executed by flexible ligand and the rigid receptors. The grid box size *x, y*, and *z* values are 114 × 92 × 82, and the grid box the center *x, y*, and *z* values are 2.2544 x −4.967 × 6.213 with a grid spacing of 0.651 Å at the binding site for 3F81 protein. The protein preparations of 3F81 for molecular docking calculations were achieved on Auto Dock-Vina software. Co- crystallized ligands, waters and co-factors were removed before preparing protein for docking. To calculate Kollman charges and polar hydrogen's, the Auto Dock Tools (ADT) graphical user interface was used. The Lamarckian Genetic Algorithm (LGA) feature in Auto Dock software was utilized for docking process [29]. The isolated compound namely STML ligand structures were drawn by ChemDraw 12.0 software. The synthesized 2D compound structures were changed into mol format that was further converted into the 3D the structure by Auto Dock software was utilized for docking process; all these ligands were purified and prepared by Auto Dockligand-input tools via selected torsion tree-choose root and torsion tree-detect root. The purified final ligands were saved via output-save as pdbqt format for further use in molecular docking studies. The outcome results of visualization were performed by using Discovery Studio software [30].

## 3. Results and discussion

### 3.1. Structural elucidation of isolated compound

The isolated compound from the leaves of *A.muricata* is confirmed to be (STML) was given in Fig. 1, having steroidal nucleus by the positive tests shown for Salkowski, Libermannbuchard reactions, and the test for alcohol [31]. The stigmasterol is a white crystalline solid [10] with a melting point of 169 °C [32]. A similar white crystalline solid of STML is isolated from the same gene *Annona glabara* L. The mixture of solvents utilized for the isolation is listed in Table 1.

The retention time of STML isolated from the methanolic extract of *Annona muricata* leaves was about 3.707, which matches with the report of [33] as shown in Fig. 2. The peak area and retention time of isolated STML are listed in Table 2. The outcomes achieved for this study are confirmed by the data reported ear-

**Fig. 2.** High-performance liquid chromatography (HPLC) image of isolated compound of STML.

**Table 2**
Peak area and retention time of isolated STML from HPLC analysis.

| Peak | Ret.Time | Area | Height | Area% | Height% |
|---|---|---|---|---|---|
| 1 | 2.387 | 78,542 | 1501 | 0.539 | 0.396 |
| 2 | 3.707 | 10,292,942 | 309,120 | 70.623 | 81.467 |
| 3 | 4.821 | 4,202,913 | 68,822 | 28.838 | 18.138 |
| Total | 10.9761 | 14,574,397 | 379,443 | 100.00 | 100.00 |

lier on the detection of STML in *Annona glabara* L. plant extracts [11]. GC–MS analyses of phytoconstituents in plants provide a clear picture of their fragmentation pattern and molecular formula. In our present investigation, GC-MS studies confirmed the molecular weight of the isolated compound as 412 with the molecular formula $C_{29}H_{48}O$ [12]. The presence of STML is confirmed by the GCMS spectrum as shown in (Fig. 3) and peak area and retention time are listed in Table 3. In addition, the physical and analytical data of the isolated compound (STML) is summarized in Table 4.

### 3.2. DFT calculations

Molecular electrostatic potential (MEP) is a significant tool to better understand the relative polarity and reactivity of a molecule [34,35]. MEP is also useful for detecting and investigating molecular interactions such as hydrogen bonding, drug-receptor interactions, and enzyme-substrate interactions. The optimized structures at B3LYP/6–311++$G$ (d,p) level of theory are used to generate MEPs of the isolated compound STML was displayed in Fig. 4. The various values of the electrostatic potential at the surface are represented by various colors. The color-coding of the MEP surface can be given as red region is electron-rich (electrophilic reactive center); blue region is an electron-deficient region (nucleophilic reactive center); yellow is a slightly electron-rich region and green are neutral. The potential increases in the order of red < orange < yel-

low < green < blue. STML molecule displays high negative electron density around the hydroxyl group attached to OH of (O20) oxygen atom owing to the lone pair of electrons. As a result, these areas are associated with electrophilic reactivity. Other areas with strong positive electron density, as illustrated in, are associated with nucleophilic reactivity represented in Fig. 4. These results provide information concerning the region where the compound can interact with hydrogen bonding molecularly. By displaying the values in a manifold of the spatial position surrounding the molecule, such a depiction gives more precise information about electrostatic potential dispersion.

The dipole moments (Debye) of the title compound STML is presented in Table 5, indicating that the dipole moment of this title compound could support more interaction with high dipole moment species, especially in biological systems [36,37]. The energy of the highest occupied molecular orbital ($E_{HOMO}$) and the lowest unoccupied molecular orbital ($E_{LUMO}$) is used for future research. Frontier molecular orbitals (FMOs) are a very important tool for studying molecular interactions inside a compound. The HOMO provides an electron as electron donor and the LUMO receives electrons as an electron acceptor. The ionization potential (I) and electron affinity (A) of the molecule is determined by values of $E_{HOMO}$, $E_{LUMO}$, and $E_{HOMO\text{-}LUMO}$ energy gap (eV), respectively. The lower value of HOMO and LUMO energy gap (eV) confirms that the compound is extra polarized, active, and has little kinetic bioactivity [38]. Global chemical reactivity describes the hardness ($\eta$), chemical potential ($\mu$), softness (s), electronegativity ($\chi$) and electrophilicity index ($\omega$), and is defined by HOMO and LUMO energy values for a molecule [39]. Based on $E_{HOMO}$ and $E_{LUMO}$, these are calculated using the below equations.

Utilizing Koopmann's theorem for closed-shell molecules.

The hardness of the molecule $\eta = (I - A)/2$      (1)

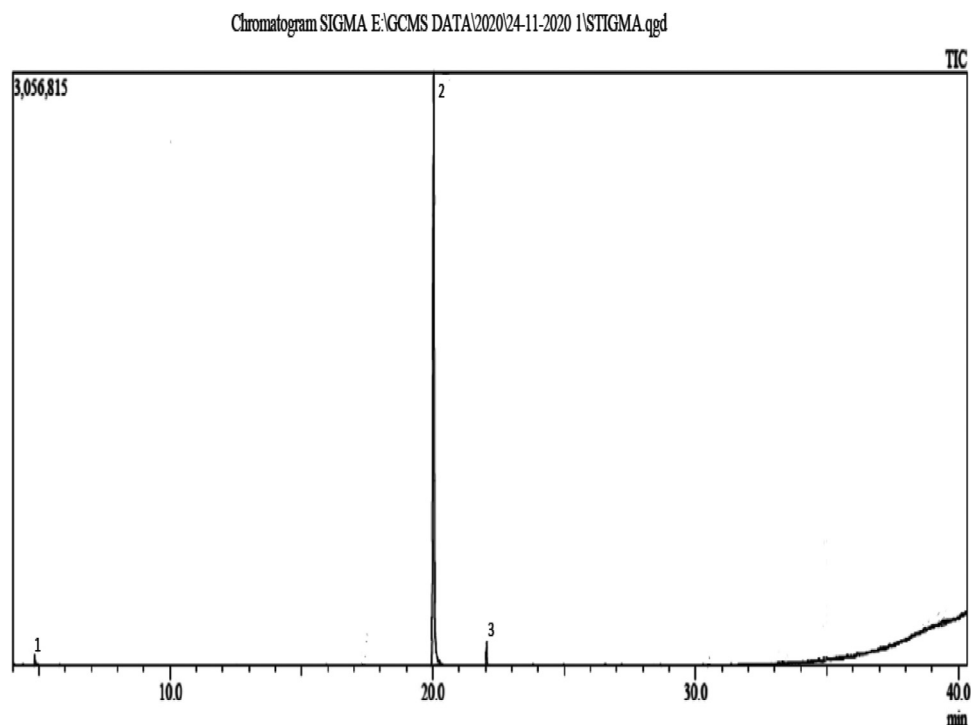Chromatogram SIGMA E:\GCMS DATA\2020\24-11-2020 1\STIGMA.qgd



**Fig. 3.** GC–MS analysis results of isolated STML compound.

**Table 3**
Peak area, retention time (RT) and name of isolated compound of (STML) from GCMS analysis.

| Peak | (RT) | Start time | End Time | m/z | Area | Area% | Height | Height% | A/H | Name |
|------|------|------------|----------|-----|------|-------|--------|---------|-----|------|
| 1 | 4.84 | 4.82 | 4.955 | TIC | 133,904 | 1.16 | 54,979 | 1.33 | 2.44 | 2-Diethyla minoethanol |
| 2 | 20.4 | 20.98 | 20.46 | TIC | 82,091 | 87.9 | 76,663 | 67.73 | 10.7 | Stigmasterol (STML) |
| 3 | 23.4 | 23.36 | 23.35 | TIC | 144,069 | 0.15 | 28,550 | 0.25 | 5.05 | Campesterol |

**Table 4**
The physical and analytical data of the isolated compound STML.

| Compounds | Molecular formula (Molecular.wt.) | %C Calcd | %H Calcd | %N Calcd | % O Calcd | Melting Point °C |
|-----------|-----------------------------------|----------|----------|----------|-----------|------------------|
| STML | $C_{29}H_{48}O$ (412.37) | (Found) 84.40 (84.25) | (Found) 11.72 (11.62) | (Found) – – | (Found) 3.88 (3.54) | 168- 169 |

**Table 5**
The calculated frontier orbital energies, $\chi$, $\mu$, $\omega$, I, A, $\eta$ and S of the isolated compound STML using B3LYP/6–31G++ (d,p) levels.

| Parameters | B3LYP/6–31G++(d,p) |
|------------|---------------------|
| SCF energy (a.u) | −1208.897 |
| Dipole moment (Debye) | 2.4095 |
| $E_{HOMO}$ (eV) | −6.3183 |
| $E_{LUMO}$ (eV) | −0.5419 |
| $\Delta E_{GAP}$ (eV) | 5.7764 |
| I (eV) | 6.3183 |
| A (eV) | 0.5419 |
| $\chi$ (eV) | 3.4299 |
| $\mu$ (eV) | −3.4301 |
| $\eta$ (eV) | 2.8882 |
| S (eV) | 0.3463 |
| $\omega = \mu^2/2\eta$ | 2.0413 |

The Ionization potential $I = -E_{HOMO}$ (2)

The electron affinity $A = -E_{LUMO}$ (3)

The chemical potential of the molecule $\mu = -(I + A)/2$ (4)

The softness of the molecule $S = 1/\eta$ (5)

The electronegativity of the molecule $\chi = (A + I)/2$ (6)

The electrophilicity index of the molecule $\omega = \mu^2/2\eta$ (7)

The ionization potential (A) and an electron affinity (I) of our isolated compound STML calculated by the B3LYP/6–311G++(d,p) method are −0.5419 (eV) and −6.3183 (eV) respectively, and the energy difference between HOMO-LUMO Gap (eV) computed at the DFT level value of 5.7764 is shown in Fig. 5. We can deduce the reactivity and stability of molecules from educating the chemical hardness and global softness. The smallest (greater) value of hardness (softness) will be the reactivity. From Table 5, it is found that the STML compound exhibited a low value of chemical hardness $\eta$(eV) value of 2.8882 and a high value of global softness S (eV) value of 0.3463. Therefore, this isolated STML compound
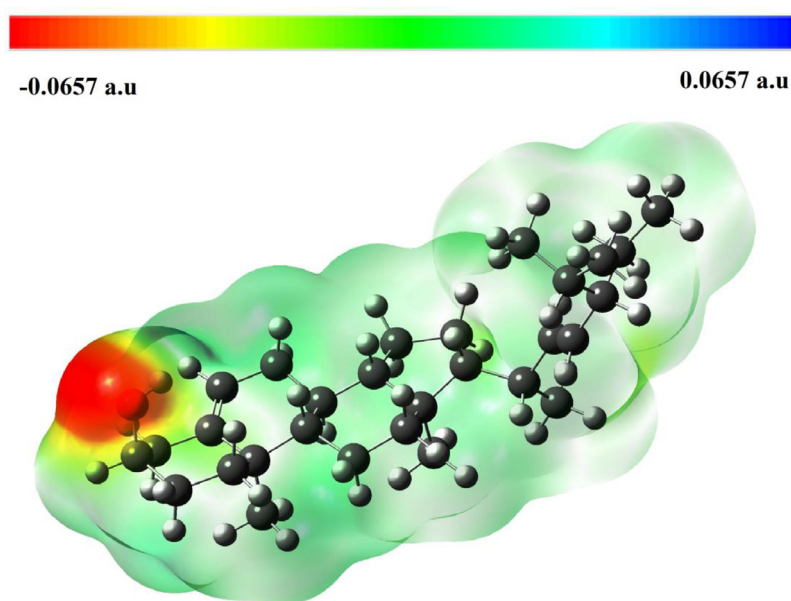
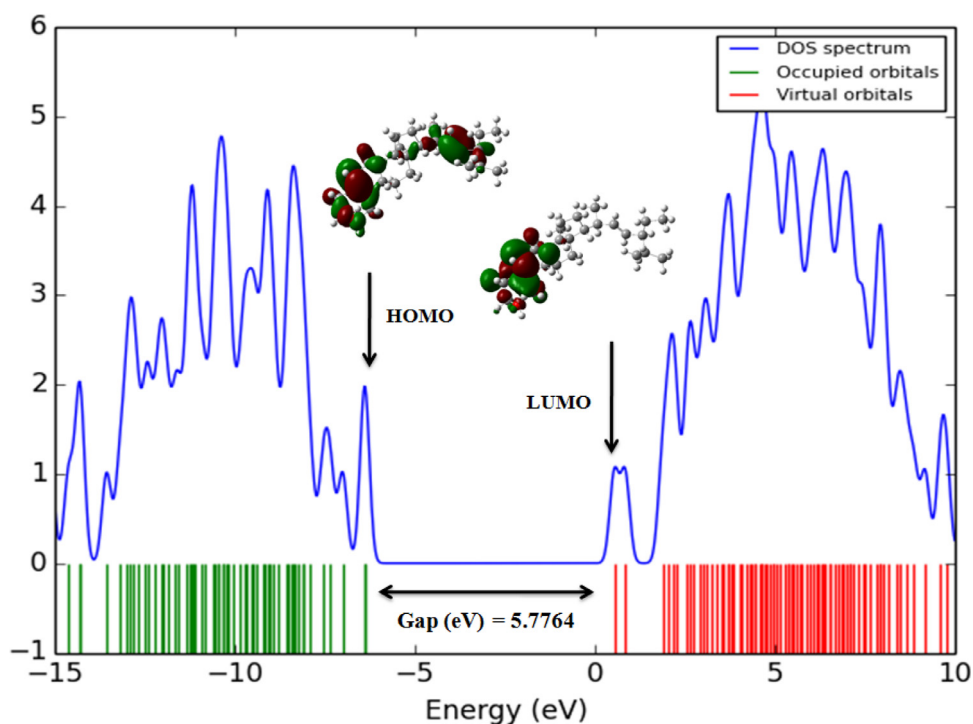**Fig. 4.** MEP surface of STML.



**Fig. 5.** Calculated TDOS spectrum of the isolated compound STML.

is chemically reactive. Furthermore, the lowering in the HOMO and LUMO energy gap describes the crucial charge transfer interactions that occur within the molecule and also possesses very good chemical with biological activities [40]. The Gauss-Sum 3.0 Program [22] was used to calculate the character of the molecular orbitals (HOMO-LUMO energy) and prepare the total density of the states (TDOS) plot as shown in Fig. 5. The DOS plot displays population analysis per orbital and provides a clear picture of the composition of molecular orbitals in a certain energy range. Fig. 5 presented (HOMO-LUMO) represented by the

red color is denoted as the positive phase and the green color is denoted as the negative phase. It is visible from the figure that, the HOMO levels diffuse mainly over octahydronaphthalen-2-ol, (E)−5-ethyl-2-methylhept-3-ene, and are partially presented in the octahydro-1H-indene group. LUMO levels are diffuse mainly over the octahydronaphthalen-2-ol group.

Four optimized step numbers are obtained in the potential energy curve analysis method using the DFT/B3LYP method with a 6−311++G (d, p) basis set for the isolated compound STML exhibited in Fig. 6. The calculated self-consistent field (SCF) energy is
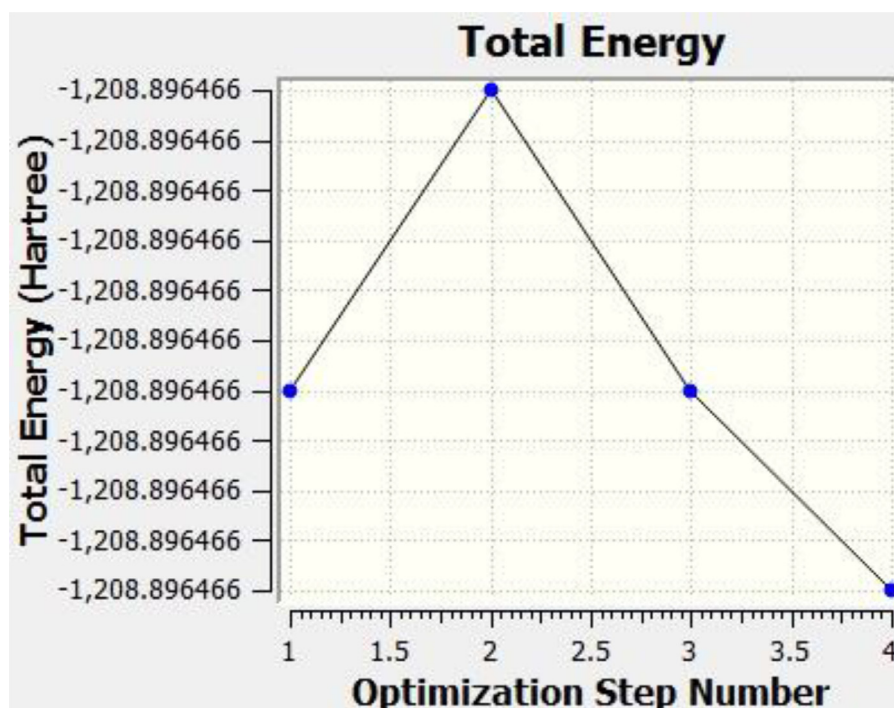
**Fig. 6.** Potential energy curve using DFT/B3LYP method with 6–311++$G$ (d, p) basis set for the isolated compound STML.
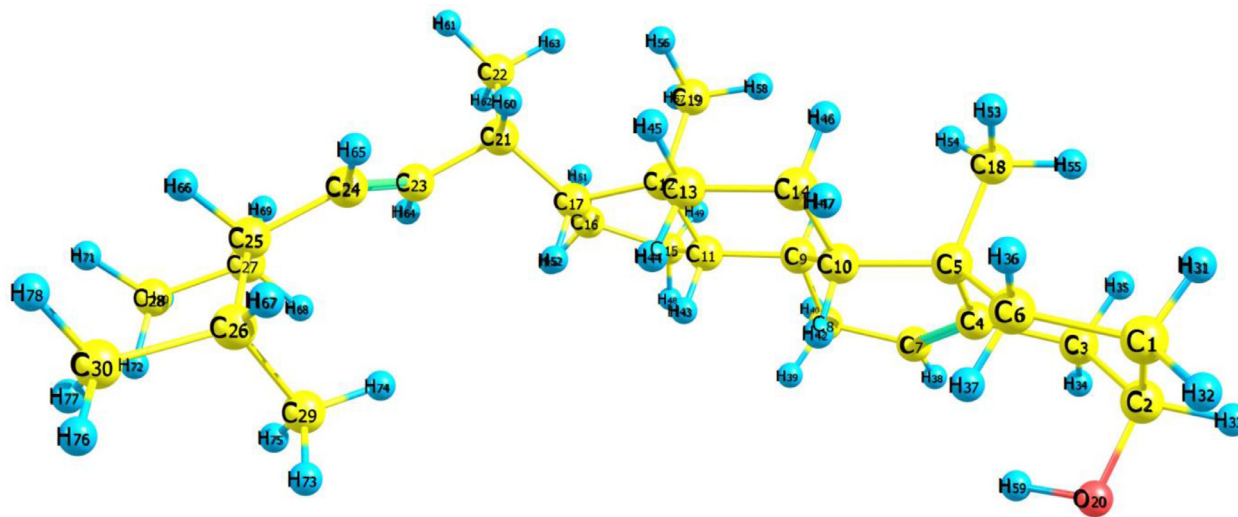


**Fig. 7.** Optimized structure of the isolated compound STML.

−1208.897 a. u. which is shown in Table 5. Fig. 7 shows the optimized structure of the isolated compound STML in Table S1 and Table S2 present their bond lengths and bond angles computed using an optimized structure basis set of 6–311G++ (d, p) by the DFT method. The optimized structure proved a mild modification in the calculated C−C bond distances in the octahydronaphthalen-2-ol group, such as C1-C2, C1-C6, C2-C3, and C3-C4, respectively, to their values of 1.535, 1.540, 1.539, and 1.522A$^0$. The excellent outcome of various bond lengths, respectively, C5-C6, C5-C10, C16-C17, C25-C26, and C25-C27 bonds are significantly greater than any other C−C bond. The C−O bond length (C2-O20) distance is 1.467 A$^0$ and the $\beta$−hydroxyl group of the O−H bond length (O20-H59) distance is 0.981 A$^0$ which is lower bond distance value than (C2-O20). The O−H bond length is less than 1 A$^0$, so it will guide to obtaining highly bioactive behavior of this isolated compound STML. For example, C56-C19-H58 and H57-C19-H58 bond angles computed at 107.20 and 107.20° as well as another one, C26-C29-H74 and C26-C30-H78 bond angles computed at 111.10 and 111.10° were incredibly optimized for the structure by the DFT/B3LYP method with 6–311++$G$ (d, p) basis set for the isolated compound STML. The (C−C−O) bond angles of different C1-C2-O20 and C3-C2-O20 values of 110.90 and 110.50°. These values are nearly the same as the $\beta$−hydroxyl group of (O−H) bond angles of different O20-C2-H33 and C2-O20-H59 values of 104.30 and 109.00° as seen in Table S2.

The calculated reactive atomic charges are crucial in the application of quantum mechanical calculations in the molecular system. STML Mulliken atomic charges are presented in Table S3 and shown in Fig. 8. Mulliken atomic charges are computed by the DFT/B3LYP method using the 6–311++$G$ (d,p) basis set. As can be seen in Table S3, H59 with all hydrogen atoms in addition to C2, C4, and C12 atoms has a net positive charge. However, O20
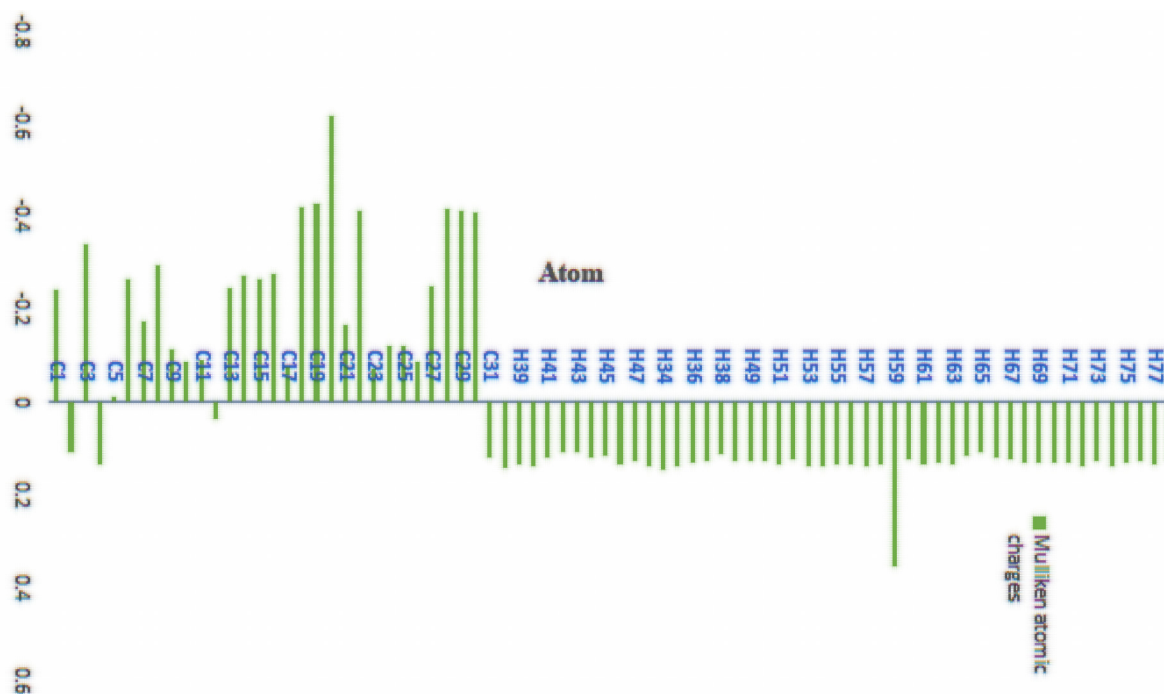
**Fig. 8.** Mulliken atomic charge distribution of STML.*3.3. Spectroscopic characterization.*

**Table 6**

Theoretical and experimental electronic absorption spectra values of using TD-DFT/6–311G++(d,p) method and their assignments.

| Name | Experimental (EtOH) $\lambda_{max}$ (nm) | Transition Occurred | Band gap (eV) | Theoretical (gas phase) $\lambda_{max}$ (nm) | Band gap (eV) | Oscillator strength (f) | Assignment |
|------|------|------|------|------|------|------|------|
| STML | 270 | $n \to \pi^*$ | 6.325 | 264.45 | 6.476 | 0.0701 | HOMO → LUMO (49.17%) |

the negative charge is positioned on the O20 atom, which is the donor atom, in addition to the net positive charge on hydrogen atoms, which are acceptor atoms. The donor and acceptor atoms may suggest the existence of intermolecular hydrogen bonding in the bioactivity of the molecule.

The Ultraviolet (UV) and $^1$H and $^{13}$C nuclear magnetic resonance (NMR) spectroscopy characterization studies were carried out with the experimentally and theoretically *ab* initio Density functional theory (DFT) method at the B3LYP level with a 6–311++$G$ (d,p) basis set [17–19].

### 3.3. Ultraviolet-Visible spectral analysis

The UV absorption spectra can detect the intensity of light detected from the sample. The experimental and theoretical UV–Visible spectrum of the isolated compound STML was recorded in ethanol (EtOH) as a solvent Fig. 9a and Fig. 9b. The theoretical UV-Visible spectrum was computed (TD-DFT/6–31 $G$ ++(d,p) basis set) using (gas phase). The computed absorption spectrum exhibits that the greater range of UV-Visible absorption wavelengths complies with the (HOMO→ LUMO) electronic transition with a (49.17%) contribution to STML. The theoretical UV-Visible spectrum of STML was plotted with the Gauss Sum 3.0 program. Time-dependent DFT can predict the excited state of properties like bandgap energy. The experimental and predicted electronic properties of electronic transitions, notably the absorption wavelength (λ), excitation energy (E), and oscillator strengths (f), are depicted in Table 6. The experimental maximum absorption ($\lambda_{max}$) value of 270 nm (in EtOH) showed excellent concord with their theoretical absorption values of 264.45 nm (in the gas phase). These excitations indicate that the n→π* transition occurs in STML isolated compound and

it shows a hypsochromic shift. The energy of the bandgap was estimated by the formula, $E = hc/\lambda$. Here, h and c are constant; λ is the cut-off wavelength [41,42].

### 3.4. $^{13}$C and $^1$H NMR spectral studies

The NMR spectroscopy confirmed the structure and molecular deal with STML. The DFT computation of NMR shielding was quick and appropriate for the great system. In the present study, the DFT method for the analysis of empirical $^1$H and $^{13}$C data of the isolated STML compound; the $^1$H and $^{13}$C chemical shifts were calculated in STML (CDCl$_3$) as a solvent with a B3LYP/6–311++$G$ (d, p) basis set by the GIAO program [43] and theoretically calculated NMR results are well deal with the experimental data.

The authors modified the program's absolute shielding in chemical shifts by subtracting the absolute shielding of tetramethylsilane (TMS). Calculated chemical shift values and experimentally measured data are listed for $^{13}$C NMR shown in Table S4 and $^1$H NMR existing in Table S5. The isotropic shielding data was developed for the assessment of the isotropic chemical shifts $\delta$ with reference to TMS. $\delta_{iso}(X) = \sigma_{TMS}(X)- \sigma_{iso}(X)$, where $\delta_{iso}$ isotropic chemical shift plus $\sigma_{iso}$-isotropic shielding. The $^{13}$C NMR Chemical Shifts, Absolute Shielding TMS values are 182.4572 and 31.6297 for $^1$H NMR spectra. The DFT/B3LYP/6–311G++(d,p) $^1$H and $^{13}$C NMR graphical representation of the isolated compound STML is shown in Fig. S1.

Fig. S2 shows the $^{13}$C NMR spectra of the isolated compound. In our current research, this isolated molecule of STML was inspected through both experimental and theoretical aspects with the DFT/B3LYP/6–311G++(d,p) basis set. In the $^{13}$C NMR spectrum,
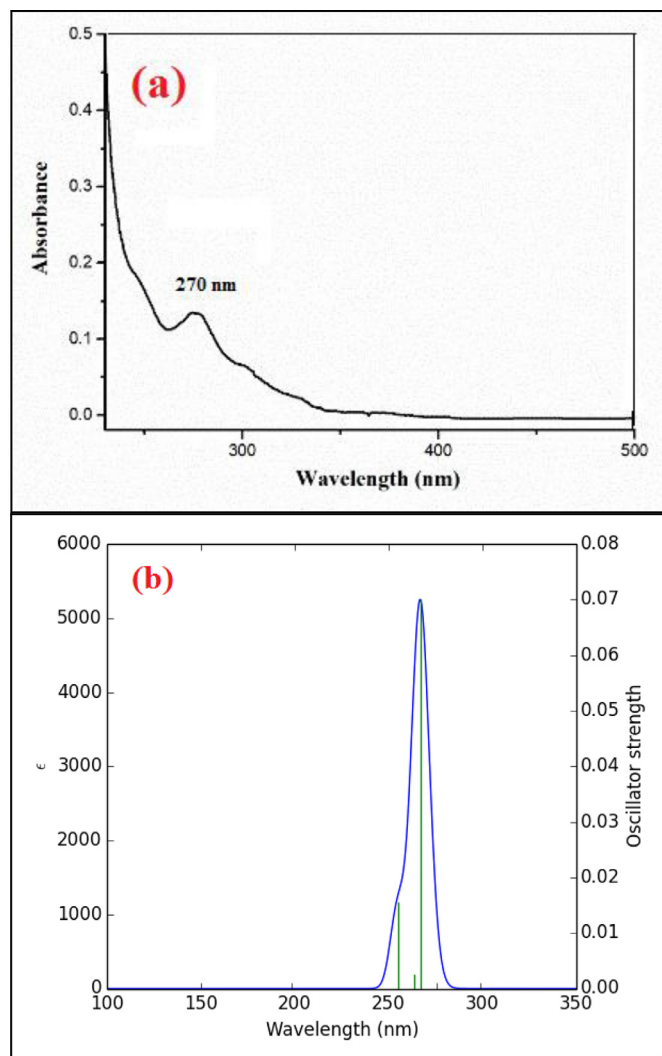
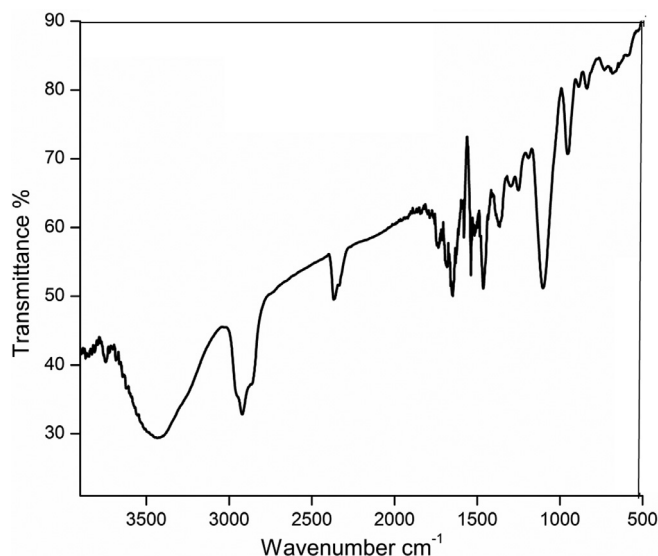**Fig. 9.** (a) Experimental and (b) theoretical UV-Visible spectra of STML.



**Fig. 10.** FT-IR Spectra of the isolated compound of STML.

STML peaks were observed (experimentally) in the region from 12.275 to 140.996 ppm, whereas their respective peaks predicted (theoretically) were in the region from 11.858 to 143.719 ppm. Each peak in the ^{13}C NMR spectrum identifies a carbon atom in a different environment within the molecule. The ^{13}C NMR spectra of the isolated compound exhibit Methyl (-CH$_3$) carbons such as C28, C22, C29, and C30 observed chemical shift values of $\delta$ 12.275, 19.621, 21.303, and 21.436 ppm, which are located in the (E)−5-ethyl-2-methylhept-3-ene group and also found a good deal with the predicted chemical shift values of $\delta$ 11.858, 18.879, 22.309, and 23.144 ppm. Other methyls (-CH$_3$) carbons such as C19 and C18 observed chemical shift values of $\delta$ 12.457 and 19.208 ppm, which are located in the octahydro-1H-indene ring with excellent agreement with the predicted chemical shift values of $\delta$ 12.033 and 16.073 ppm. Methylene (-CH$_2$) carbons such as C27 were predicted at $\delta$ 24.447 ppm, which is located in the (E)−5-ethyl-2-methylhept-3-ene group and observed at $\delta$ 24.593 ppm. The Methylene carbons in the order of C15, C16, and C13 carbons were predicted at $\delta$ 25.374, 29.889, and 39.839 ppm which is signified in the octahydro-1H-indene ring and observed at $\delta$ 25.622, 29.129, and 39.923 ppm. The octahydronaphthalen-2-ol ring containing Methylene carbons such as C1, C8, C6, and C3 carbon was predicted at $\delta$ 32.212, 32.089, 36.989, and 42.356 ppm and observed at $\delta$ 32.106, 32.139, 36.754, and 42.459 ppm. Both theoretical and experimental analysis STML provided an excellent deal with Methylene (-CH$_2$) carbons. The cyclohexane C5 carbon was predicted of $\delta$ 37.498 ppm giving a superior agreement with the observed value at $\delta$ 37.347 ppm; it was presented in the octahydronaphthalen-2-ol ring. Cyclopentane C12 carbon was predicted at $\delta$ 42.551 ppm and shows excellent concord with observed value at $\delta$ 46.642 ppm; it was identified in the octahydro-1H-indene ring.

The C26, C21, and C25 methane (-CH) carbons were located in the (E)−5-ethyl-2-methylhept-3-ene group. They were predicted at $\delta$ 31.812, 41.975, and 54.518 ppm and provided a wonderful deal with the observed chemical shift values at $\delta$ 31.909, 40.695, and 51.469 ppm. The Octahydro-1H-indene rings containing C10, C17, and C11 carbons were predicted at $\delta$ 48.422, 54.518, and 58.034 ppm. They are in concord with the observed values at $\delta$ 50.412, 56.211, and 57.109 ppm. The signal was found at $\delta$ 72.038 ppm, which confirmed the (C2) $\beta$-hydroxyl group of carbon was the occurrence of an octahydronaphthalen-2-ol ring and also exhibited an amazing agreement with the predicted value at $\delta$ 73.452 ppm. STML shows distinguishable signals were observed at $\delta$ 140.996 and 121.931 ppm that are assigned to C4 and C7 double bonds in the cyclic structure of the octahydronaphthalen-2-ol ring and revealed amazing concordance predicted values at $\delta$ 143.719 and 120.305 ppm. The signal was detected at $\delta$ 129.531 and 138.528 ppm, indicating an external double bond between C23 and C24 carbons that were the presence of (E)−5-ethyl-2-methylhept-3-ene group and also exhibited superior agreement with the predicted values at $\delta$ 129.386 and 138.089 ppm as seen in Table S4.

Fig. S3 ^{1}H NMR spectra of isolated compound STML exhibited proton signals in ppm. These chemical shift values were observed (experimentally) in the region from 0.699 to 5.490 ppm, whereas their respective peaks predicted (theoretically) were in the region from 0.617 to 5.628 ppm.

The ^{1}H NMR spectra of the isolated compound STML have six methyl (-CH$_3$) protons, four methyl protons respectively, (H70, H71, H72), (H73, H74, H75), (H76, H77, H78), and (H6, H7, H8) hydrogen atoms were observed chemical shifts value ranges at $\delta$ 0.964–0.995 ppm and the predicted chemical sifts value ranges at $\delta$ 0.916–1.032 ppm, which are signifies (E)−5-ethyl-2-methylhept-3-ene group. The (E)−5-ethyl-2-methylhept-3-ene group containing methyl protons of (H61, H62, H63) and the octahydronaphthalen-2-ol ring containing methyl protons of (H53, H54, H55) with their
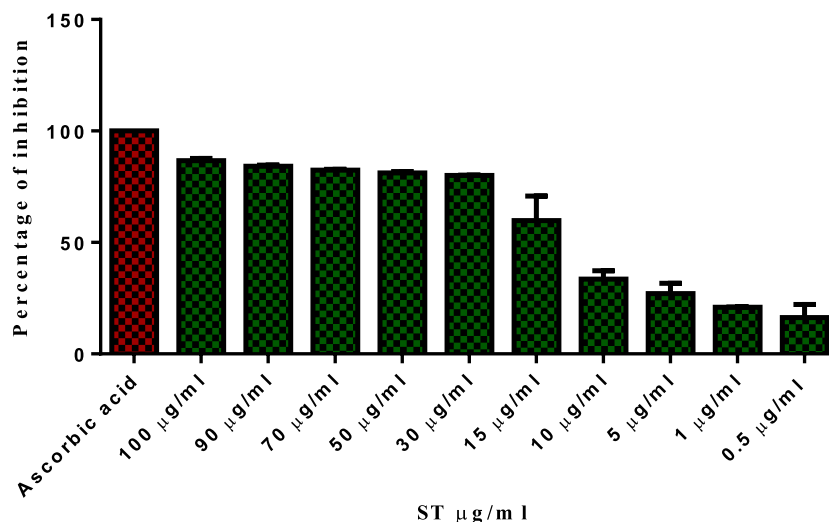
**Fig. 11.** The Radical scavenging activity of the compound STML as expressed in percentage of Inhibition by ABTS assay (data were calculated as the mean ± SD of three measurements and represented along with the error bar).

observed chemical shift values at $\delta$ 1.124–1.137 ppm and predicted chemical shift values at $\delta$ 1.033 - 1.096 ppm, these six methyls (-CH$_3$) protons revealed that the observed chemical shifts values are well-suited with the predicted chemical shift values. The eight methylene (-CH$_2$) protons were confirmed by the $^1$H NMR spectrum of the isolated compound of STML. Two methylene protons of (H44, H45) and (H46, H47) hydrogen atoms observed chemical shift signals revealed at $\delta$ 1.150–1.192 and 1.390–1.383 ppm with predicted chemical shift values at $\delta$ 1.129–1.169 and 1.344–1.373 ppm, which are located in the octahydro-1H-indene ring. The Octahydronaphthalen-2-ol ring containing two methylene protons of (H39, H40) and (H34, H35) hydrogen atoms observed chemical shift signals revealed at $\delta$ 1.754–1.796 and 1.863–1.959 1.390–1.383 ppm with predicted chemical shift values at $\delta$ 1.727–1.756 and 1.1.855–1.999 ppm. The two octahydro-1H-indene rings of (H48, H49), (H50, H51) methylene protons, and one octahydronaphthalen-2-ol ring containing methylene proton revealed the observed chemical shifts value ranges at $\delta$ 1.495–1.636 ppm and predicted chemical shifts value ranges at $\delta$ 1.497–1.668 ppm. Finally, one (E)−5-ethyl-2-methylhept-3-ene group-containing (H68, H69) methylene proton observed chemical shifts value ranges at $\delta$ 1.305–1.318 ppm and the predicted chemical shift value ranges at $\delta$ 1.315–1.328 ppm. These eight methylene (-CH$_2$) protons discovered that the observed chemical shifts values are a good deal better than the predicted chemical shift values.

Seven methane (-CH) protons were verified by the $^1$H NMR spectrum of the isolated compound STML. Three methane protons observed chemical shift values at (H43 atom; $\delta$ 0.699–0.757 ppm), (H41 atom; $\delta$ 0.810–0891 ppm), and (H52 atom; $\delta$1.233–1.240 ppm) with predicted chemical shift values at (H43 atom; $\delta$ 0.617–0.759 ppm), (H41 atom; $\delta$ 0.788 −0.886 ppm), and (H52 atom; $\delta$ 1.217–1.246 ppm), which are denoted in the octahydro-1H-indene ring. Three methane hydrogen such as (H33), (H41), and (H42) protons signals are observed chemical shift value range at $\delta$ 2.006–2.213 ppm were located in the octahydronaphthalen-2-ol ring and predicted chemical shift value range at $\delta$ 2.274 - 2.653 ppm. Finally, one methane hydrogen (H66) chemical shift value was observed at $\delta$ 1.404–1.418 ppm and the predicted chemical shift value was at $\delta$ 1.407–1.448 ppm. These seven methane (-CH) protons exhibited that the observed chemical shifts values are well-matched with the predicted chemical shift values.

The $\beta$−hydroxyl (-OH) proton was denoted the octahydronaphthalen-2-ol ring containing (O20- H59) bond observed chemical shift values at (H59 atom; $\delta$ 3.407–3.437 ppm) with predicted chemical shift values at (H59 atom; $\delta$ 3.187 - 3.697 ppm), which are good agreement with the observed and predicted $^1$H NMR chemical shift values. The two ethylene (H64-C23 = C24-H65) protons were presented by the $^1$H NMR chemical shift values observed at (H64 and H65 atoms; $\delta$ 5.225–5.235 ppm) and predicted chemical shift values at (H64 and H65 atoms; $\delta$ 5.022 - 5.118 ppm) and another one ethylene (-C4 = C7 - H38) proton was confirmed by the $^1$H NMR chemical shift value observed at (H38 atom; $\delta$ 5.465–5.490 ppm) and also predicted the chemical shift value at (H38 atom; $\delta$ 5.532 - 5.628 ppm). These three ethylene protons were illustrated amazing-deal with both observed and predicted $^1$H NMR chemical shift values as seen in Table S5.

### 3.5. Fourier-transform infrared (FTIR) spectral analysis

The FTIR spectra of the isolated compound are shown in Fig 10. The bands indicate the presence of hydroxyl, alkenes, methyl, and methylene groups. The broad band at 3423.65 cm$^{-1}$ is attributed to OH stretching. The peak at 2920.23 cm$^{-1}$ corresponds to the presence of aliphatic C–H stretching, sharp band at 1101 cm$^{-1}$ signifies the presence of cycloalkane. The absorption band at 1658 cm$^{-1}$ is attributed to the C–C stretching band of the C=C double bond. A week band at 1463 cm$^{-1}$ is the bending frequency of cyclic CH$_2$ stretching and 1249 cm$^{-1}$ for CH$_2$ (CH$_3$)$_2$These data match with the data available in the literature [44–46].

### 3.6. Biological sections

In the present study, we evaluated the effect of the isolated compound of STML from *Annona muricata* Linn leaves on scavenging ABTS (2,2′-azino-bis (3-ethylbenzthiazoline-6-sulfonic acid) assay radicals. From a calibration curve with R equal to 0.9691, we calculated the antiradical power of compound STML, which is expressed in μg equivalent of ascorbic acid per milligram and their results are presented in Fig. 11.

The ABTS (2,2′-azino-bis(3-ethylbenzthiazoline-6-sulfonic acid) assay is another widely used *in vitro* radical scavenging test. However, this method requires the generation of ABTS radicals, which
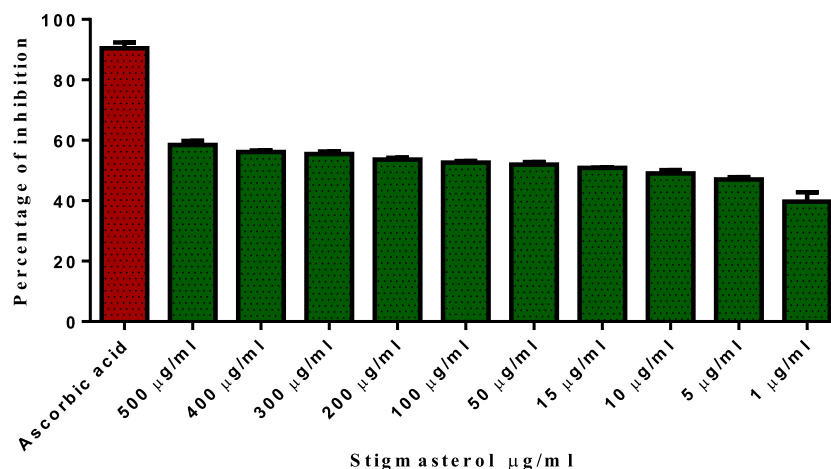
**Fig. 12.** DPPH radical scavenging activity of isolated compound of STML from *Annona muricata Linn* leaves using ascorbic acid as a standard.
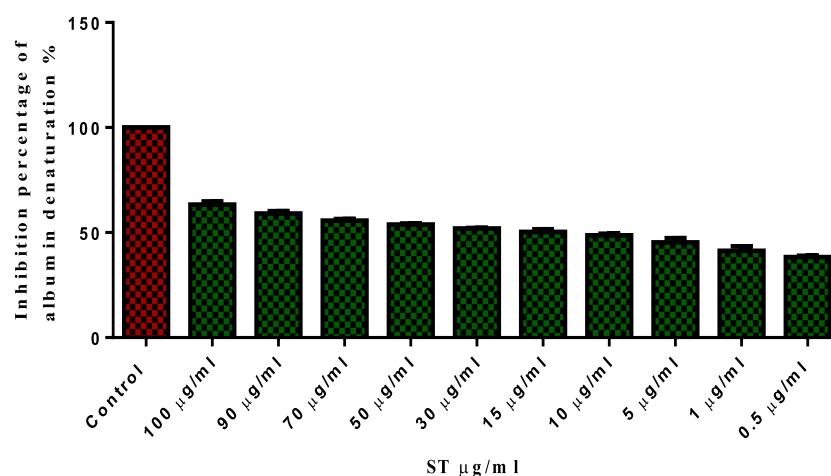


**Fig. 13.** Anti-inflammatory activity of the tested isolated compound of STML from *Annona muricata* Linn leaves. Data are presented as mean values $\pm$ standard deviation ($n = 3$).

can be easily achieved by reacting ABTS salt with potassium persulfate. The ABTS radical action is reactive towards most antioxidant compounds. The radical ABTS is soluble in both aqueous and organic solutions. The ABTS technique may be used to assess the antioxidant capacity of lipophilic and hydrophilic antioxidants in a variety of materials, including plant extracts. A compound having the property of giving electrons will reduce the ABTS blue-green radical solution to a colorless neutral form [47]. In the case of the isolated compound of STML, we distinguish that the best antiradical activity observed of the $IC_{50}$ of STML was found to be 13.41 μg/ml. The maximum antioxidant activity was observed for the compounds at 100 μg/ml exhibiting a scavenging activity of 86.63% whereas, for the standard ascorbic acid, it showed an activity of 100%.

In this investigation, the DPPH degrading properties of formulated powder were increased in a dose-dependent manner. The functional isolated compound of STML from *Annona muricata* Linn leaves exhibited a maximum DPPH scavenging trait with an $IC_{50}$ value of 14.73 μg/ml. The maximum antioxidant activity was observed for the compounds at 500 μg/ml, exhibiting a scavenging activity of 58.48% whereas, for the standard ascorbic acid, it showed an activity of 90.42% Fig. 12. Values are the mean of experiments performed in triplicate and data is expressed as mean $\pm$ SD. The dose-response for the anti-inflammatory activity of the compound STML is displayed in Fig. 13. The compound exhibited anti-inflammatory activity with the $IC_{50}$ value of 17.59 μg/ml un-

der a non-linear fit of transform of concentration *versus* response analysis (r2 = 0.9164). At the concentration of 100 μg/ml, the anti-inflammatory activity was exhibited with a mean value of 63.36% whereas, for the control drug Acetylsalicylic acid, the heat denaturation of proteins to 100% was shown at 100 μg/ml.

In the current research, an isolated compound of STML from *Annona muricata* Linn leaves was calculated for its *in vitro* cytotoxicity activity against HeLa and Vero, the normal (fibroblast) cell lines. The functional isolated compound STML depicted strong anticancer attributes against both the HeLa and Vero cell lines with cells viabilities at a higher concentration of 100 μg/ml, 30% of cells were viable and observed to be unaffected. It was highly nontoxic at 0.5 μg/ml with 60% of viable cells. Similarly, in Vero cell lines at a concentration of 500 μg/ml, 71.94% of cells were obtained to be viable Fig. 14 and Fig. 15. Hence, the determined $IC_{50}$ value of the compound STML in Vero cells was found to be 173.8 μg/ml by MTT assay Fig. 16a and Fig. 16b. Similar study reports about the cell cytotoxicity of plant extracts were discussed [48,49].

### 3.7. In silico molecular docking studies

In our present studies, the isolated molecule of stigmasterol (STML) from the ethanolic extracts of *Annona muricata* leaves was discovered to have significant *in vitro* anticancer activity in cervical cancer (HeLa) cell lines at a higher concentration of 100 μg/ml, 30% of cells were viable and observed to be unaffected. As a result, this
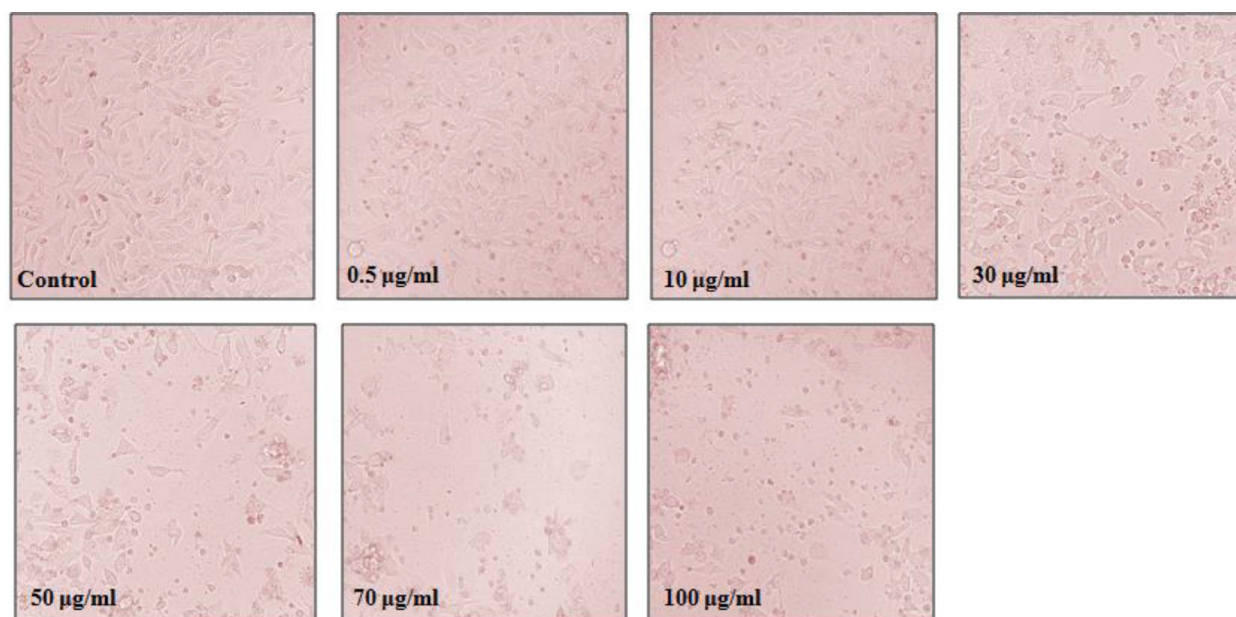
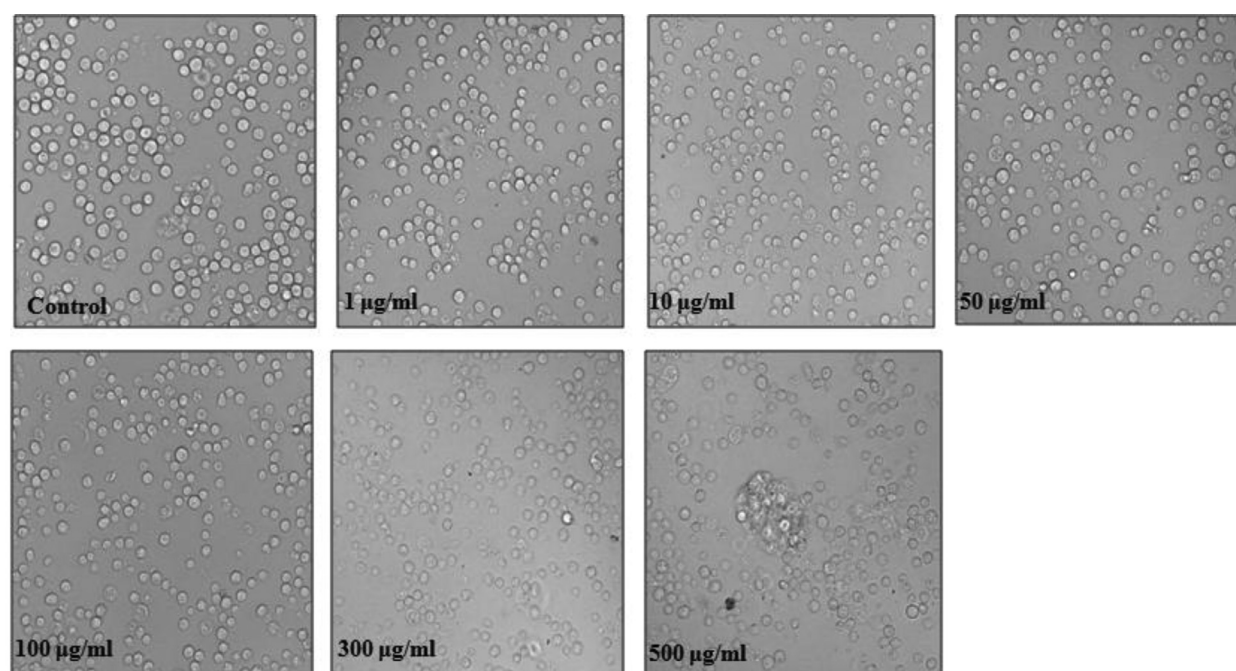**Fig. 14.** Anticancer activity of He La (Cervical cells).



**Fig. 15.** Anticancer activity of Vero cells.

isolated molecule was analyzed further in silico molecular docking analysis against the Multidentate small-molecule inhibitors of vaccinia H1-related (VHR) phosphatase decrease proliferation of cervix cancer cells (RCSB PDB ID: 3F81), which was achieved and downloaded from the RCSB PDB formatted protein target [28]. Cell cycle arrest is caused by the receptor of (3F81) VHR phosphatase in HeLa carcinoma cells, indicating that VHR inhibition may be an effective method to preventing the development of cancer cells, including squamous intraepithelial lesions and squamous cell carcinomas of the uterine cervix. This led us to believe that VHR may be a unique and potential therapeutic target for cervical cancer therapy [50] and those small-molecule inhibitors of VHR must be important tools to validate this novel target. VHR is typically up-

regulated in several cervix cancer cell lines as well as in uterine cervix carcinomas, and researchers have reported the development of multidentate small-molecule inhibitors of VHR that inhibit its enzymatic activity at nanomolar concentrations and demonstrate anticancer properties on cervix cancer cells. The inhibitors inhibited the proliferation of cervical cancer cells while having no effect on the development of primary normal keratinocytes. As a result, this isolated (STML) molecule might be used to produce medicines to treat for cervical cancer.

In the docking procedure, a protein target for molecular docking experiments was chosen as *vaccinia* H1-related (VHR) phosphatase (PDB ID: 3F81). Table S6 shows the binding affinity and inhibition
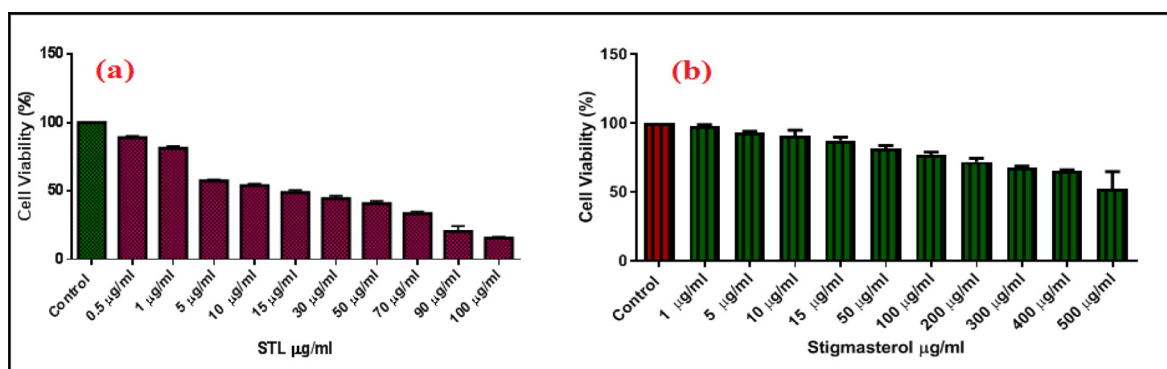
**Fig. 16.** (a) *In vitro* cytotoxicity effects on Hela Cells and (b) Vero Cells of isolated compound of STML from *Annona muricata* Linn leaves.
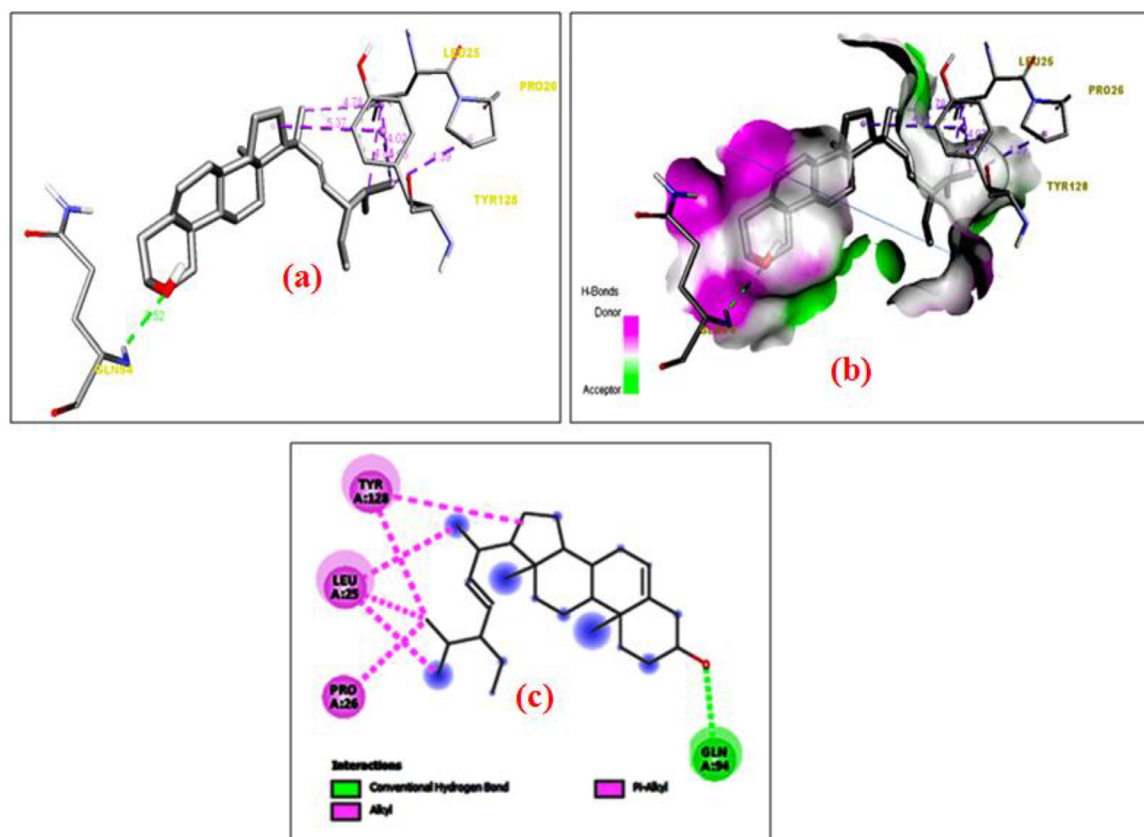


**Fig.17.** (a) Hydrogen bond Interaction of STML ligand with 3F81 protein. (b) Hydrogen bond Receptor-side surface Interaction of STML ligand with 3F81protein. (c) 2D-Hydrogen bond Interaction representation of STML ligand with 3F81 protein.

constant $K_i$ of all resultant ligands. The results suggest that all the STML could strongly occupy the active location of 3F81.

The docking analysis of (ligand-receptor) interaction is given in Table S7. The 3F81 protein with STML ligand is detected to have a good binding energy value of −6.6(kcal/mol), and a 14.34816 μM inhibition constant ($K_i$) [51] respectively. From the docking result, it shows that the STML interacts with 3F81 with GLN94, TYR128, PRO26, and LEU25 residues that are involved in hydrogen bonding, $\pi$-alkyl hydrophobic, and alkyl hydrophobic having bond lengths of 2.52 Å, 5.37 Å, 4.05 Å, 4.38 Å, 4.02 Å, 4.77 Å, and 4.54 Å respectively.

The ligand-receptor hydrogen bond contacts, receptor side hydrogen bond interactions, and their 2D-ligand-receptor hydrogen bond interactions between STML and 3F81 are depicted in Fig. 17. It indicates stick model represents the STML. The Pink dotted line represents the $\pi$- alkyl hydrophobic, and alkyl hydrophobic bonds between binding residues and green dotted lines represent hydrogen bonding.

## 4. Experimental

For all experimental procedures and compound characterization information, please see the supplementary material relating to this article.

## 5. Conclusion

Results from the present study showed that the isolated natural bioactive compound stigmasterol (abbreviated as STML) from *Annona muricata*. Linn leaves had significantly potent cytotoxic effects on HeLa and Vero cancer cells with a high selective index when compared with that of control of Vero cell lines at various

concentrations. Hence, the plant possessed mainly fatty acids and phthalic acid derivatives with anticancer effects as well as high selectivity between cancerous and normal cells. As a consequence of their extremely selective index, it provides a novel source of anticancer drug development, with little toxicity to healthy or normal tissue in the body, as demonstrated by the findings of this study. Further, STML was studied with several analytical techniques, such as FTIR, UV–Visible spectroscopy, $^1$H, and $^{13}$C NMR. The structure of STML optimized molecular geometry, UV–Visible, and NMR chemical shifts of the compound were theoretically calculated using the DFT method, and comparison was completed with their good-deal of experimental results. The charge distribution of STML was calculated by the Mulliken population analysis. The frontier molecular orbitals (FMOs) studies, the energy difference between HOMO-LUMO Gap (eV) computed at the DFT level value of 5.7764 is shown in (Figure S4). This compound also exhibited substantial interaction energy values against the protein target vaccinia H1-related (VHR) phosphatise, reducing the proliferation of cervical cancer cells (RCSB PDB ID: 3F81) with a binding energy value of $-6.6$(kcal/mol) and a 14.34816 M inhibition constant (Ki). Future research will look into this compound's potentially anticancer properties.

## Credit author statement

J. Irshad Ahamed: Conceptualization, Supervision, *In Silico* analysis work, Spectral characterizations, *In vitro* studies, analyzing results, Writing - review & editing.

Francy. K: Methodology and computational analysis studies.

A. Vini Priya, J. PremaKumari, and R. P. Steiny: Formal analysis, Methodology.

P. Kamalarajan: Investigation Visualization.

B. Venkatadri: Anti-bacterial studies.

## Declaration of Competing Interest

We confirm that the manuscript has been read and approved by all named authors and that there are no other persons who satisfied the criteria for authorship but are not listed. We further confirm that the order of the authors listed in the manuscript has been approved by all of us.

## Supplementary materials

Supplementary material associated with this article can be found, in the online version, at doi:10.1016/j.molstruc.2021.132186.

## References

[1] P.A. Cohen, A. Jhingran, A. Oaknin, L. Denny, Lancet 393 (2019) 169–182.
[2] F.V. Zapata, A. Miranda de la Cruz, L. Magaña-Olán, J.M.G. Hernández, J.D.C. Madrigal, Eur. Sci. J, ESJ. 14 (2018) 69.
[3] O.A. Ibeanu, Cancer Biol. Ther. 11 (2011) 295–306.
[4] A. Mitra, D.A. MacIntyre, J.R. Marchesi, Y.S. Lee, P.R. Bennett, M. Kyrgiou, Microbiome. 4 (2016) 1–15.
[5] C. Vora, S. Gupta, ESMO Open 3 (2018) e000462.
[6] D.K. Gaffney, Hashibe M, D. Kepka, K.A. Maurer, T.L. Werner, Gynecol. Oncol. 151 (2018) 547–554.
[7] L. Kma, Asian Pac. J. Cancer Prev. 14 (2013) 3429–3436.
[8] M. Greenwell, P.K.S.M. Rahman, Int. J. Pharm. Sci. Res. 6 (2015) 4103–4112.
[9] H. Ali, S. Dixit, D. Ali, S.M. Alqahtani, S. Alkahtani, S. Alarifi, Drug Des Devel Ther. 9 (2015) 2793–2800.
[10] A. Edilu, L. Adane, D. Woyessa, Ann. Clin. Microbiol. Antimicrob. 14 (2015) 1–8.
[11] T. Matsumoto, S. Watanabe, R. Kawamura, K. Taguchi, T. Kobayashi, Life Sci. 118 (2014) 200–205.
[12] R. Rajesh, N. Jaivel, P. Marimuthu, Res. J. Med. Plant. 8 (2014) 646–656.
[13] M.R. Habib, F. Nikko, M. Rahman, M.E. Haque, M.R. Karim, Pak. J. Biol. Sci. 10 (2007) 4174–4176.
[14] A. Kamboj, A.K. Saluja, Int. J. Pharm. Pharma. Sci. 3 (2011) 94–96.
[15] S. Karthikeyan, K. Kalaimurugan, A. Prathima, Energy sources a: recovery util, Environ. Eff. 39 (2017) 2046–2052.
[16] M.J. Frisch, G.W. Trucks, H.B. Schlegel, G.E. Scuseria, M.A. Robb, J.R. Cheeseman, G. Scalmani, V. Barone, B. Mennucci, G.A. Petersson, H. Nakatsuji, Revision D. 01, Wallingford, CT 201, Gaussian. Inc,, 2009.
[17] J. Irshad Ahamed, M. Priya, P. Vinothkumar, K. Sathyamoorthy, P. Murali-Manohar, J. Liu, M.F. Valan, J. Mol.Struct. 1202 (2020) 127241.
[18] J. Irshad Ahamed, M.F. Valan, K. Pandurengan, P. Agastian, B. Venkatadri, M.R. Rameshkumar, K. Narendran, Res. Chem. Intermed. 47 (2021) 759–794.
[19] J. Irshad Ahamed, G.R. Ramkumaar, P. Kamalarajan, K. Narendran, M.F. Valan, T. Sundareswaran, T.A. Sundaravadivel, B. Venkatadri, S. Bharathi, J. Mol. Struct (2021) 131418.
[20] M.K. Abdel-Latif, H.R. Abd El-Mageed, H.S. Mohamed, F.M. Mustafa, J. Mol. Struct. 1200 (2020) 127056.
[21] P. Ramesh, M.L. Caroline, S. Muthu, B. Narayana, M. Raja, S. Aayisha, J. Mol. Struct. 1200 (2020) 127123.
[22] N.M. O'Boyle, A.L. Tenderholt, K.M. Langner, J. Comp. Chem. 29 (2008) 839–845.
[23] R. Robereta, P. Nicoletta, P. Anna, P. Ananth, Y. Min, R. Catherine, J. Free Radic. Biol. Med. 26 (1999) 1231–1237.
[24] K. Shimada, C.J. Jong, K. Takahashi, S.W. Schaffer, Taurine 9 (2015) 581–596.
[25] Y. Mizushima, M. Kobayashi, J. Pharm. Pharmacol. 20 (1968) 169–173.
[26] S. Sakat, A.R. Juvekar, M.N. Gambhire, Int. J. Pharm. Pharm. Sci. 2 (2010) 146–155.
[27] J.X. Zhang, H. Wei–Tan, C.Y. Hu, W.Q. Wang, G.H. Chu, L.H. Wei, L. Chen, Exp. Ther. Med. 15 (2018) 2575–2582.
[28] xxx 2021 https://www.rcsb.org/structure/3F81.
[29] G.M. Morris, D.S. Goodsell, R.S. Halliday, R. Huey, W.E. Hart, R.K. Belew, A.J. Olson, J. Comput. Chem. 19 (1998) 1639–1662.
[30] Visualizer, Discovery Studio, Accelrys Software Inc, Dis. Stud. Vis. 2 (2005).
[31] P. Pratheema, S. Gurupriya, B.K. Sahira, L. Cathrine, World J. Pharm. Pharm. Sci. 6 (2017) 1872–1885.
[32] P.S. Nayak, D.M. Kar, P.N. Shweta, Int. J. Pharm. Pharma. Sci. 7 (2015) 25–29.
[33] K. Manjula, K. Rajendran, T. Eevera, S. Kumaran, J. Liq. Chromatogr. Relat. Technol. 36 (2013) 197–212.
[34] J. Lee, T. Park, S. Jeong, K.H. Kim, C. Hong, Bioorg. Med. Chem. Lett. 17 (2007) 1284–1287.
[35] J.F. Beattie, G.A. Breault, R.P. Ellston, S. Green, P.J. Jewsbury, C.J. Midgley, J.E. Pease, Bioorg. Med. Chem. Lett. 13 (2003) 2955–2960.
[36] Y.S. Cho, M. Borland, C. Brain, C.H.T. Chen, H. Cheng, R. Chopra, S. Kim, J. Med. Chem. 53 (2010) 7938–7957.
[37] D.A. Abdelrheem, A.A. Rahman, K.N. Elsayed, H.R. Abd El-Mageed, H.S. Mohamed, S.A. Ahmed, J. Mol. Struct. 1225 (2021) 129245.
[38] U. Klingmüller, M. Schilling, S. Depner, L.A. D'Alessandro, Elsevier Inc (2013) 45–64.
[39] H.M. Jesudoss, M. Saminathan, R.E. Jesudoss, D. Murugan, P. Alagusundaram, Braz. J. Phys. 1 (2018) 28–43.
[40] M. Alcolea Palefox, Int. J. Quantum Chem. 77 (2000) 661–684.
[41] M. Raja, R.R. Muhamed, S. Muthu, M. Suresh, J. Mol.Struct. 1128 (2017) 481–492.
[42] S.M. Hiremath, A. Suvitha, N.R. Patil, C.S. Hiremath, S.S. Khemalapure, S.K. Pattanayak, V.S. Negalurmath, K. Obelannavar, S.J. Armaković, S. Armaković, Spectrochim. Acta A. 205 (2018) 95–110.
[43] R. Ditchfield, Mol. Phys. 27 (1974) 789–807.
[44] O.T. Osuntoku, T.O. Idowu, M.C. Gamberini, Biochem. Pharmacol. 7 (2018) 1–9.
[45] G. Padmasri, D.V.L. Sarada, J. Pharm. Res. 4 (2011) 3601–3602.
[46] M. Xianghe, P. Qiuyue, L. Yun, Eur. Food Res. Technol. 235 (2012) 1039–1047.
[47] O.C. Okou, S.E.S. Yapo, K.E. Kporou, E.L. Baibo, S. Monthaut, A.J. Djaman, J. Appl. Biosci. 122 (2018) 12282–12290.
[48] R. Sukirtha, K.M. Priyanka, J.J. Antony, S. Kamalakkannan, R. Thangam, Gunasekaran P, M. Krishnan, S. Achiraman, Process Biochem. 47 (2012) 273–279.
[49] K. Murugan, K. Dinesh, K. Kavithaa, M. Paulpandi, T. Ponraj, M.S. Alsalhi, S. Devanesan, J. Subramaniam, R. Rajaganesh, H. Wei, S. Kumar, Parasitol. Res. 115 (2016) 1085–1096.
[50] R. Henkens, P. Delvenne, M. Arafa, M. Moutschen, M. Zeddou, L. Tautz, J. Boniver, T. Mustelin, S. Rahmouni, BMC Cancer 8 (008) (2021) 1–9.
[51] M. Gümüş, Y. Sert, A. Yalkın, H. Gökce, I. Koca, Chem. Sel. 4 (2019) 4695–4708.